

# Experimental and Theoretical Characterization of Sand-Carrying by Heavy Oil-Flow in a Horizontal Wellbore

Hong Gao, Zhiming Wang, Xiaoqiu Wang, Dongying Wang

Wellbore Complex Flow and Well Completion Lab, China University of Petroleum, Beijing, China

## Email address:

563848102@qq.com (Hong Gao), wellcompletion@126.com (Zhiming Wang), 13466396559@126.com (Xiaoqiu Wang),

1396769578@qq.com (Dongying Wang)

## To cite this article:

Hong Gao, Zhiming Wang, Xiaoqiu Wang, Dongying Wang. Experimental and Theoretical Characterization of Sand-carrying by Heavy Oil-Flow in a Horizontal Wellbore. *International Journal of Oil, Gas and Coal Engineering*. Vol. 6, No. 6, 2018, pp. 201-213.

doi: 10.11648/j.ogce.20180606.22

**Received:** November 13, 2018; **Accepted:** December 4, 2018; **Published:** January 18, 2019

---

**Abstract:** The world's heavy oil reserves are very large. With the wide application of heavy oil cold recovery technology, the problem of blockage in oil well caused by the deposition of sand in the wellbore is becoming more and more serious. Therefore, it is very important to study the deposition and migration of sand in the wellbore. Based on indoor full-sized experimental apparatus simulating multiphase complex flows, the sand-carrying capacity of heavy oil in pipes is determined using a high-viscosity white oil and water mixture as the fluid medium, and by varying parameters such as the saturation, sand volume concentration, viscosity of heavy oil, and flow. A complete investigation is performed to obtain the basis of the sand flow in pipes and sand-bed development and migration. It is shown that the viscosity of heavy oil, main flow rate, and water content have a significant effect on the sand-carrying capacity of heavy oil, while the effect of the wall inflow on the pressure drop of the wellbore is relatively less. Based on the examination of the experimental flow pattern, an oil–water–sand-bed three-layer pressure drop model with a variable-mass flow is established for the first time. The minimum energy method is used to calculate the model. The model considers the diffusion of solid-phase particles and pressure drop by the fluid of the sand bed in heavy oil and is verified against the pressure drop data obtained from the experiments. The results show that the model is within an average relative error of 12.69%, which is satisfactory for practical engineering. Furthermore, the model provides a theoretical support for reasonable sand production in heavy oil reservoirs.

**Keywords:** Solid/Liquid Two-Phase Flow, Reasonable Sand Production, Sand-Carrying, Variable-Mass Flow, Flow Pattern

---

## 1. Introduction

Approximately 40% of the oil production wells in the world is affected by the problem of sanding production, one of the major challenges in oil production. [1] Until now, sand control techniques have been mainly applied for the exploitation of heavy oil reservoirs. Although these have received some success, they fail to eliminate sand production and have a negative impact on the well productivity. Furthermore, frequent sand control operations lead to a loss in production time, and sand control tools are expensive. In contrast to the problems mentioned above, according to the data obtained from the Bohai oilfield, [2] reasonable sand production can improve single well productivity. Thus, the optimal production strategy can be chosen by establishing the trade-off

between sand control and sanding by optimizing the sand production and well productivity. Briefly, reasonable sanding is a technique that allows a reservoir to sand limitedly and selectively. Specifically, sands with different grain sizes migrate along with oil during the process of exploitation of unconsolidated cemented reservoirs. Based on the understanding of the variation in the particle size and its distribution, grains with diameters larger than the threshold value are prevented from migrating with the oil. These blocked sands get accumulated and form sand filtration barriers. Regarding the application to heavy oil cold production, well blocking and even abandonment of a well caused by sanding are becoming increasingly serious issues. [3, 4] Thus, research on the sand-carrying capacity of oil and water flow in pipes has become even more crucial.

The experimental research on this solid–liquid two-phase

flow can be classified into three types: (1) Solid–liquid two-phase flow in a pipe. [5-7] Several solid materials such as pulverized coal and sand are transported by the water in pipes. Water is usually used as the fluid medium during the experimental simulation of this type of flow and has a high displacement. [8–11] (2) Solid–liquid two-phase flow in an annulus. [12-18] Rock cuttings are transported from the bottom of a hole to the ground in an annulus between the wall of a well and casing pipe during well drilling. Water, owing to its high displacement in the experiment, is used to model the drilling mud to simulate this type of flow. [18–21] (3) Open channel flow. [22-25] Sediment movement in a river can be regarded as an open channel flow. The Yellow River Water Conservancy Committee conducted experimental research to study the variation in the sediment water concentration in the Yellow river. Water with its high pump displacement was also used as the fluid material to simulate the flow in their experiments.

In a word, water or light oil is usually used as the fluid material in experiments to study the sand-carrying capacity in a common pipe. [6-12] Since the viscosity of water and light oil is more smaller than the viscosity of the heavy oil; besides when the heavy oil and water mixed as a fluid medium in pipes, the emulsification phenomenon will occur. When sand added, the solid-liquid mixed flow, the tube appears in the phenomenon is not the same, so the results cannot be used to

determine the basis of the sand-carrying capacity of the heavy oil flow in production pipes. So a detailed experimental research simulating heavy oil and sand flow in production pipes has been performed. However, limited by space and equipment, this experiment did not take changing of temperature into account.

In this work, a set of experimental equipment considering the variable-mass flow in horizontal wells is designed to simulate the production process of heavy oil in wells. The sand-carrying laws are acquired by varying the parameters that affect the sand-carrying capacity. This strategy is combined with the theories of complex flow in a pipe to develop a prediction model of the sand-carrying capacity of the oil and water complex flow in a pipe. Experimental data is used to verify the accuracy of the model, and the basis of the sand-bed migration understood through the experiments is also applied to achieve moderate sand production.

## 2. Experimental

### 2.1. Materials

Materials of this work, mainly including tap water, different viscosity of white oil, different mesh of sand. The properties for white oil and crude oil in experiments will be showed in part 2.3, and other parameters involved are showed in table 1.

*Table 1. Experimental materials and parameters.*

operating parameters	Experiment data	unit
dip angel	0	
mainflow	5, 10, 15, 20, 25, 30, 35, 40	m <sup>3</sup> /h
inflow	0.4, 0.8, 1.2, 1.6, 2.0, 2.4, 2.8, 3.2, 4.0	m <sup>3</sup> /h
pressure	1	Atm
temperature	15	°C
water content	10, 30, 50, 70, 90	%
viscosity of white oil	37, 150, 320	mPa.s
sand volume concentration	0.01, 0.02, 0.03, 0.04, 0.05	%
diameters of sands	20-50, 50-100, 100-150	mesh

### 2.2. Experimental Setup

This experiment is conducted on an indoor full-sized equipment simulating the oil–gas–water multiphase complex flow in the Wellbore Complex Flow and Well Completion Laboratory of China University of Petroleum. [26-28] The experimental setup included four parts: well simulation loop, experimental flowing object supply and control system, pressure acquisition and processing system, and solid–liquid separation equipment.

#### (1) Well simulation loop

The experimental loop is composed of full sized pipes made of plexiglass, and it includes three parts: 3.0-m long developing flow pattern part, 2-m long stable flow pattern part, and 2.5-m long viewing part, as shown in Figure 1. The screw holding perforation is distributed on the stable flow pattern part. The perforation density is 12 hole/m, perforation diameter is 0.01 m, and perforation phase angle is 45°.

Pressure taps are located at the entrance side and export sides of the stable flow pattern part. The pressure taps are connected to the pressure acquisition system, and the pressure drop can be examined in real time. There are two sampling points at the entrance and export sides of the stable flow pattern part. The developing flow pattern and viewing parts are connected by flanges. The reason plexiglass pipes are used is that it is easy to observe the flow characteristics and flow pattern visually and clearly. Furthermore, it is convenient to capture images of the flow pattern by a high-speed camera during the experiments.

#### (2) Experimental flowing object supply and control system

The experimental flowing object supply and control system included two screw pumps, two control cabinets, a water storage tank, and an oil storage tank. The functions of this system were providing the fluid in the experimental loop, applying pressure, and controlling the flow rate. The water and oil storage tanks were used to generate fluid circulation.



Figure 1. Horizontal variable-flow simulator.



Figure 2. Pressure acquisition and processing system.

### (3) Pressure acquisition and processing system

The pressure acquisition and processing system includes

pressure gauges and a computer on which a pressure drop acquisition and processing software is installed, as shown in Figure 2. The pressures generated at the two ends of the stable flow pattern part are applied consistently to the receiving end via pressure sensors with a certain frequency and are displayed on the computer visually. This data can be exported and saved by the processing software directly.

### (4) Solid-liquid separation equipment

Sands are filtered by the solid-liquid separation equipment as the oil and water circulated. The equipment includes a sand setting box, large column tank, screw pump, and centrifugal pump.

## 2.3. Experimental Procedure

The experiment design mainly involved ascertaining the experiment sensitive parameters, such as wellbore main flow rate, wall flow rate, oil viscosity, particle size, and water concentration. The sands setting, migration laws, and flow pattern variation as a function of the flow rate were required to be examined. Simultaneously, the height of the sand-bed and pressure drop at the stable flow pattern part were needed to be determined in real time.

1).  $0.056 \text{ m}^3$  of water was added to  $0.5 \text{ m}^3$  of white oil having a viscosity of  $37 \text{ mPa} \cdot \text{s}$ . The water volume concentration of the liquid mixture was 10%. The main flow rate was varied from 1 to  $40 \text{ m}^3/\text{h}$ .

2). Silica sand of 20–50 mesh was selected, and different quantities of sand were added so that the sand volume concentration of the mixture varied from 0.01 to 0.05%. The changes in the flow pattern and sand movement pattern were observed during the process of adjustment.

The sand was injected into the pipe by a spiral injector, controlled by a frequency converter. The specific function relationship between the sand-injection rate and rotation rate of the electrical machine in the spiral injector is shown in Figure 3.

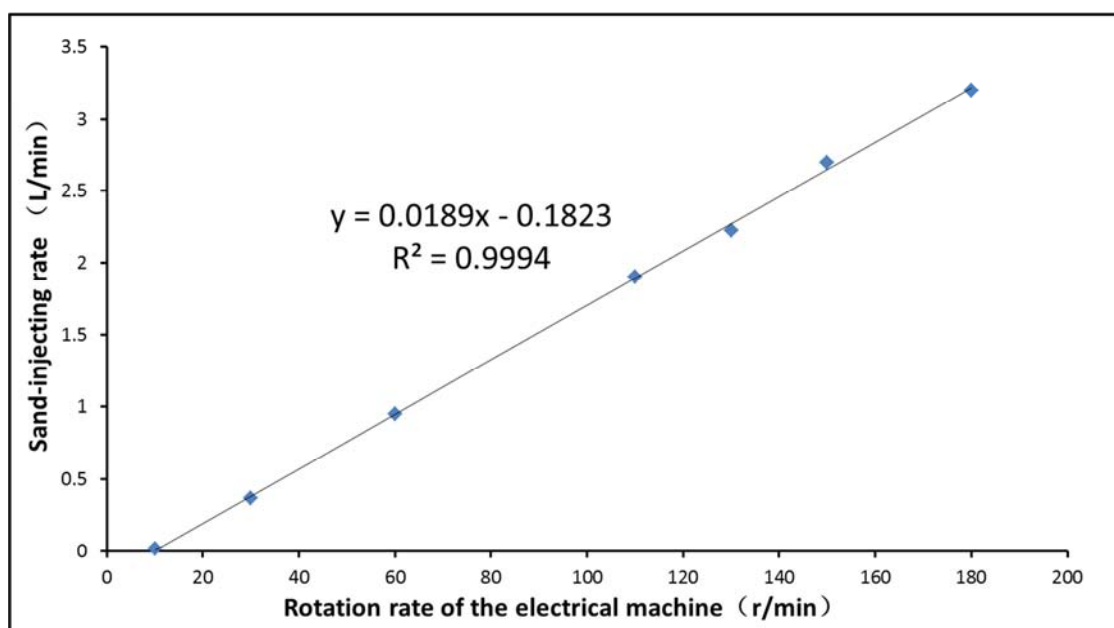


Figure 3. Function relationship between the sand-injection rate and rotation rate of the electrical machine in the spiral injector.

For a known mixture flow rate, the sand-injection rate was varied to obtain the objective sand concentration. For example, if a 1% sand concentration is required when the mixture flow rate is  $10 \text{ m}^3 / \text{h}$ , the sand-injection rate is

$$10 \times 1\% = 0.1 \text{ m}^3 / \text{h} = \frac{0.1 \times 1000}{60} \text{ L} / \text{min} \approx 1.6667 \text{ L} / \text{min}$$

Then, the rotation rate of the electrical machine in the spiral injector was calculated using the function in Figure 1. Based on the above example, the rotation rate of the electrical machine is

$$\frac{1.6667 + 0.1823}{0.0189} = 97.83 \text{ r} / \text{min}$$

The rotation rate of the electrical machine was varied by adjusting the frequency convertor.

The sand concentration was validated by measuring the volume ratio of the sand acquired from the sampling valve at the entrance section of the experimental loop.

3). The wall flow rate was adjusted so that it was in proportion to the main flow rate. Variations in the flow pattern and sand setting rules with the wall flow rate were observed. The pressure drop was measured after the wellbore flow tended toward stability. If a sand-bed was present, its height was measured.

4). Steps 2–4 were repeated using 50–100 and 100–150 mesh sands.

5). Steps 2–4 were repeated using mixtures with 30, 50, 70, and 90% water volume concentration.

For these experiments, white oil and water were mixed in a  $4\text{-m}^3$  tank in which a mixer with blades, both in the center and bottom, was used to promote homogeneity in the mixture. The following is the detailed preparation process of 30% water content mixture chosen as the representative example for a white oil and water mixture using a specific water content.

2100 L white oil and 900 L water were poured successively into the tank with the mixer.

The mixer was started, and the white oil and water were mixed for approximately half an hour.

A 500-mL graduated cylinder with the mixture sample from the sampling valve was placed at the test section of the experimental loop.

The graduated cylinder containing the mixture was kept placed for approximately 24 h so that the mixture stratified into 2 layers with the white oil layer above the water layer.

If the volumetric content of water in the mixture was approximately or exactly 30%, the corresponding mixture was regarded as the objective mixture.

If the volumetric content of water in the mixture showed a significant deviation from 30%, a longer time was required to mix the white oil and water more homogeneously.

#### 2.4. Comparison of Physical Properties of White Oil and Heavy Oil

Heavy oil is a type of crude oil having a high content of

asphaltene and resin and a high viscosity. Crude oil that has a stock tank density  $> 943 \text{ kg/m}^3$  and an underground viscosity  $> 0.5 \text{ P}$  is usually called heavy oil. The density of heavy oil usually exceeds  $860 \text{ kg/m}^3$  and its viscosity varies with temperature; therefore, heavy oil is regarded as a non-Newtonian fluid at a low temperature and a Newtonian fluid at a high temperature. Heavy oil tends to emulsify particularly when the flow velocity in a pipe is high.

White oil is a colorless and odorless liquid that is chemically inert and has a good light stability. It mainly consists of saturated hydrocarbons, and the aromatic hydrocarbon, nitrogen, oxygen, and sulfur content is extremely low. The density of white oil is  $880 \text{ kg/m}^3$ , and its viscosity varies from dozens of Pa·s to hundreds of thousands of Pa·s with temperature changing. White oil can also emulsify in some situations. In this experiment, white oil was used to substitute heavy oil as the fluid material for performing the experiments. Furthermore, it is convenient to observe the flow in the pipe with the colorless white oil and to clean the pipe. The viscosity of heavy oil required in the experiment can be prepared by different viscosities of white oil.

### 3. Experimental Phenomena and Data Processing

Accuracy of test parameters: Pressure  $\pm 0.1 \text{ Pa}$

Flow speed  $\pm 0.001 \text{ m/s}$

Moisture content  $\pm 0.1$

Main flow/inflow  $\pm 1 \text{ m}^3/\text{h}$



Figure 4. Stratified flow when the velocity of main flow is low.

In the stratified flow, as shown in Figure 4, the oil, water, and sand are divided into 3 layers when water saturation is 0.3 and main flow is  $5 \text{ m}^3/\text{h}$ . The upper layer is oil, with water in the middle layer, and sand in the bottom layer. The sand-bed is not in a stable condition as the sand from the liquid continually settles on the sand-bed. The sand-bed in the horizontal pipe is usually continuous and homogeneous, and its interface with water is smooth.

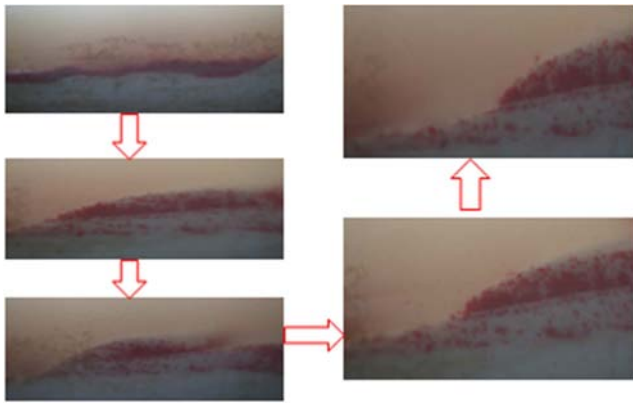


Figure 5. Sand-bed in a high velocity of main flow.



The flow pattern in Figure 5 is a dispersed oil–water flow that can be oil-in-water or water-in-oil. The sand-carrying capacity is improved when the velocity of main flow is high. The sand concentration in the sand suspension layer increases, height of the sand-bed decreases, and the bed becomes a discontinuous sand pile as can be seen in Figure 5. The sands are carried forward and out of the pipe.

Red sand is used as traceable sand in the experiments to illustrate the sand-carrying process in the pipe. The tracer sand had the same physical properties as regular sand, and its size was 50–100 mesh, matching the size of the experimental sand. Using tracer sand allowed clear observation of the movement of individual particles.



**Figure 6.** Tracer method for characterization of the sand movement.

The red sand in Figure 6 is traceable sand. It can be seen that the sand is carried as an entire sand pile when the flow velocity is low, whereas only the surface sand is carried forward with the bottom sand staying immobile when the flow velocity is high. Thus, the amount of sand produced from a reservoir should be controlled to be optimal to prevent the sand-bed from moving to the bottom of a pipe.

Water saturation is increased gradually to study its influence on the flow pattern. In the first case, the water saturation is low. The experiments revealed that as the main flow rate gradually increased, the flow pattern changed from an absolute stratified flow to a pseudo-stratified flow with oil and water dispersing in the upper layer. It becomes a water-in-oil dispersed flow as the main flow rate is further increased. In the second case, the water saturation is high. With increasing of the main flow rate, the flow pattern changes from an absolute stratified flow to a pseudo-stratified flow with oil and water dispersing in the bottom layer and pure oil in the upper layer. It becomes an oil-in-water dispersed flow when the main flow rate is further increased. In the third case, the water saturation is moderate. With increasing of the main flow rate, the flow pattern changes from an absolute stratified flow to a pseudo-stratified flow with a water-in-oil dispersion in the upper layer and oil-in-water dispersion in the bottom layer. Figures 7–9 display these flow patterns.

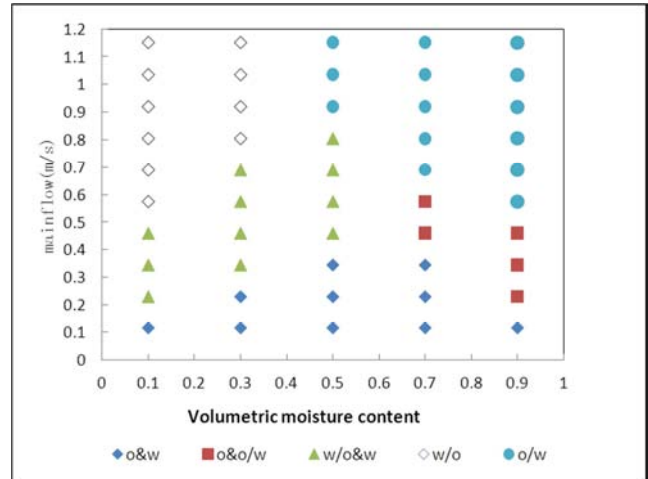


**Figure 7.** Experimental flow pattern maps for oil/water flow (inflow rate 0.4 m<sup>3</sup>/h).

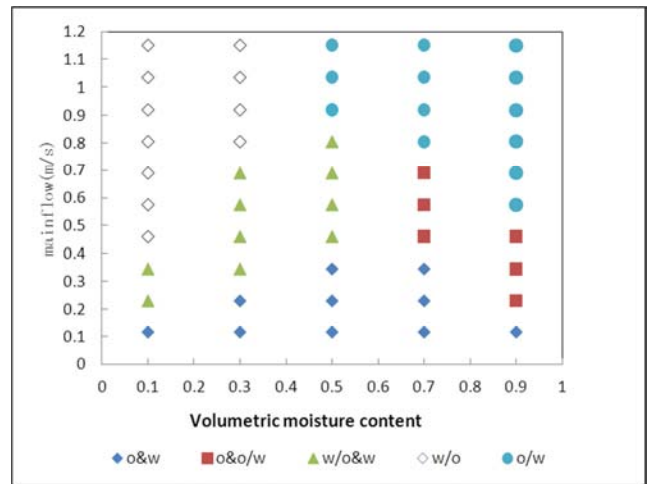


**Figure 8.** Experimental flow pattern maps for oil/water flow (inflow rate 2 m<sup>3</sup>/h).

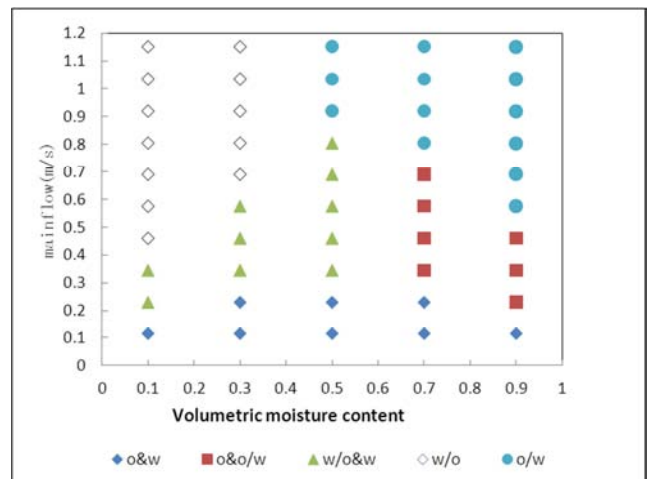


**Figure 9.** Experimental flow pattern maps for oil/water flow (inflow rate 4 m<sup>3</sup>/h).

The flow parameters are changed to examine their effect on the pressure drop. Figure 10 shows, when the main flow rate is kept constant, the pressure drop first increases and then

decreases. The turning point is called critical water saturation that is relevant for the viscosity of oil and water.

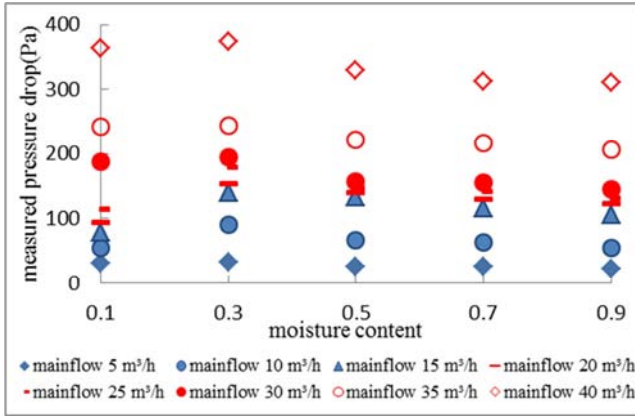


Figure 10. Measured pressure drop vs. moisture content (inflow rate 0.8 m³/h).

It can be seen from Figure 11 that the viscosity of heavy oil has a significant effect on the pressure drop; clearly, the pressure drop increases when the viscosity of heavy oil increases. It is also shown that the wall inflow has a lesser effect on the pressure drop compared with viscosity. Thus, the linear water head loss is the main part of the pressure drop in long-distance pipeline transportation.

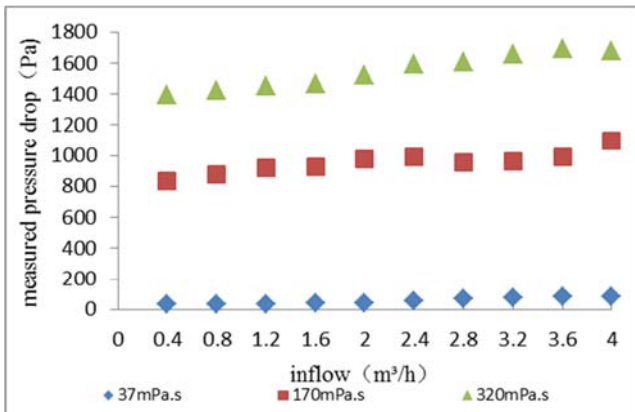


Figure 11. Viscosity of heavy oil vs. pressure drop.

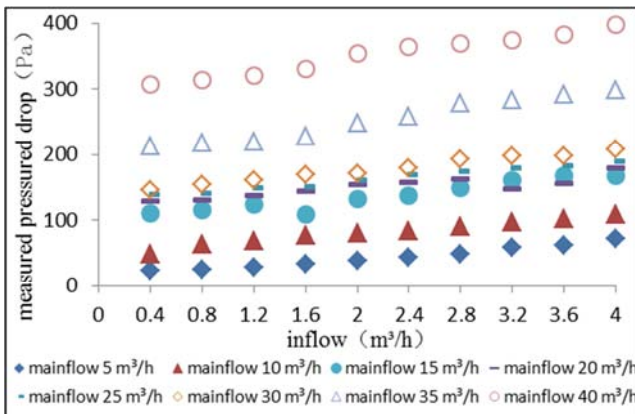


Figure 12. Variation of the pressure drop in the pipe with different wall inflows.

When the water saturation and viscosity are kept constant, the main flow rate has an obvious influence on the pressure drop, and it increases as the main flow rate increases (see Figure 12).

With increasing wall inflow, the pressure drop of the wellbore increased slowly, and it shows that the wall inflow has little effect on the pressure drop (see Figure 12).

## 4. Mathematical Formulations

### 4.1. Assumptions

The minimum cell is chosen for analysis, and because of the complex mechanism of the interaction between the solid and liquid phases, the following assumptions are in the model:

- (1) The liquid phase in the wellbore is an incompressible Newton fluid, and its petrophysical properties are continuous.
- (2) The flow in the target region is an isothermal steady flow, and there is no thermal transmission between the fluid and its environment.
- (3) The movable sand-bed is a continuous phase. Based on the experimental result in this study, the sand volume concentration was assumed as 46%.
- (4) The relative sliding between the liquid and solid phase was not considered.
- (5) The suspension phenomenon only occurs in the water layer, and there are no sands in the oil layer.

### 4.2. Hierarchical Model

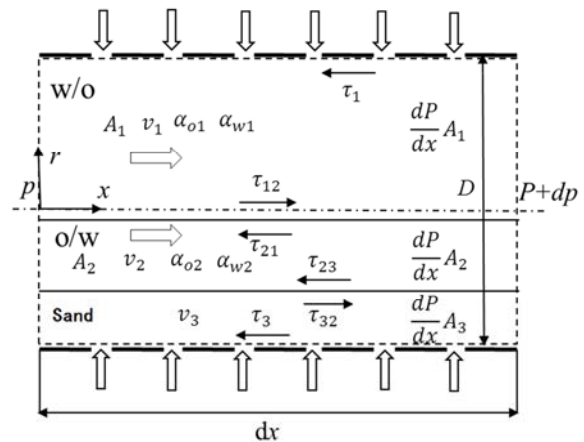


Figure 13. Control body of stratified flow model of target segment.

List the mass conservation equations for three phases:

$$\frac{dq_w}{dx} = q_{sw} \quad (1)$$

$$\frac{dq_o}{dx} = q_{so} \quad (2)$$

$$\frac{dq_s}{dx} = q_{ss} \quad (3)$$

Volume flow of oil phase, water phase and solid phase:

$$q_o = \alpha_{o1} A_1 v_1 + \alpha_{o2} A_2 v_2 + v_3 A_3 (1 - c_{mb}) \alpha_{o2} \quad (4)$$

$$q_w = \alpha_{w1} A_1 v_1 + \alpha_{w2} A_2 v_2 + v_3 A_3 (1 - c_{mb}) \alpha_{w2} \quad (5)$$

$$q_s = A_3 v_3 \quad (6)$$

Based to theory of fluid mechanics:

$$\alpha_{o1} + \alpha_{w1} = 1 \quad (7)$$

$$\alpha_{o2} + \alpha_{w2} = 1 \quad (8)$$

Substituting (6) and (8) into (4) and (5),

$$(1 - \alpha_{w1}) A_1 v_1 + \alpha_{o2} A_2 v_2 + (1 - c_{mb}) \alpha_{o2} A_3 v_3 = q_o \quad (9)$$

$$\alpha_{w1} A_1 v_1 + (1 - \alpha_{o2}) A_2 v_2 + (1 - c_{mb}) (1 - \alpha_{o2}) A_3 v_3 = q_w \quad (10)$$

$$v_3 = \frac{c_s Q}{A_3} \quad (11)$$

Assuming a wall inflow angle of 90 degrees, the momentum correction factor can take a value of 1, regardless of the fluid flow in the sand bed:

$$-\frac{d(pA_1)}{dx} - \tau_1 s_1 (1 - \phi) - \tau_{12} s_{12} = \frac{d(\rho_1 A_1 v_1^2)}{dx} \quad (12)$$

$$-\frac{d(pA_2)}{dx} - \tau_2 s_2 (1 - \phi) + \tau_{12} s_{12} - \tau_{23} s_{23} = \frac{d(\rho_2 A_2 v_2^2)}{dx} \quad (13)$$

$$-\frac{d(pA_3)}{dx} - \tau_3 s_3 (1 - \phi) + \tau_{23} s_{23} = \frac{d(\rho_3 A_3 v_3^2)}{dx} \quad (14)$$

By combining the above three formulas, the constraint equation for the stratified flow of oil-water two-phase carrying sand can be obtained:

$$\begin{aligned} (1 - \phi) \left( \frac{\tau_1 s_1}{A_1} - 2 \frac{\tau_2 s_2}{A_2} + \frac{\tau_3 s_3}{A_3} \right) + \tau_{12} s_{12} \left( \frac{1}{A_1} + \frac{2}{A_2} \right) - \tau_{23} s_{23} \left( \frac{2}{A_2} + \frac{1}{A_3} \right) \\ = 2 \left( -\rho_1 v_1 \frac{dv_1}{dx} + 2 \rho_2 v_2 \frac{dv_2}{dx} - \rho_3 v_3 \frac{dv_3}{dx} \right) \end{aligned} \quad (15)$$

Adding the formulas (12), (13), and (14), the pressure drop equation of the horizontal wellbore oil-water sand three-phase stratified flow wellbore can be obtained:

$$-A \frac{dp}{dx} = (1 - \phi) (\tau_1 s_1 + \tau_2 s_2 + \tau_3 s_3) + 2 \left( \rho_1 v_1 A_1 \frac{dv_1}{dx} + \rho_2 v_2 A_2 \frac{dv_2}{dx} + \rho_3 v_3 A_3 \frac{dv_3}{dx} \right) \quad (16)$$

The sand bed layer is not filled with solid phase sand. It has been proved by experiments that the sand bed volume concentration can be regarded as a macroporous medium, so the additional pressure drop caused by the fluid flow in the wellbore must be considered. [29-32]

Considered the sand bed as a macroporous medium, and the additional pressure drop equation generated by fluid flow. [33]

$$\frac{dp}{dx} = \left[ \frac{17.3}{\text{Re}_f} + 0.336 \right] \frac{\rho_2 c_{mb} v_{xd}^2}{d_s (1 - c_{mb})^{4.8}} \quad (17)$$

$$-A \frac{dp}{dx} = (1 - \phi) (\tau_1 s_1 + \tau_2 s_2 + \tau_3 s_3) + 2 \left( \rho_1 v_1 A_1 \frac{dv_1}{dx} + \rho_2 v_2 A_2 \frac{dv_2}{dx} + \rho_3 v_3 A_3 \frac{dv_3}{dx} \right) + A_3 \frac{\rho_2 c_{mb} v_{xd}^2}{d_s (1 - c_{mb})^{4.8}} \left[ \frac{17.3}{\text{Re}_f} + 0.336 \right] \quad (18)$$

$$\rho_1 = \rho_w \alpha_{w1} + \rho_o \alpha_{o1} \quad (19)$$

$$\rho_2 = \rho_w \alpha_{w2} + \rho_o \alpha_{o2} \quad (20)$$

$$\rho_3 = \rho_w (1 - c_{mb}) \alpha_{w2} + \rho_o (1 - c_{mb}) \alpha_{o2} + \rho_s c_{mb} \quad (21)$$

The frictional stress is calculated using the concept of

Among them, the fluid Reynolds Number  $\text{Re}_f = \frac{\rho_2 v_2 d_2}{\mu_2}$ ,

Relative velocity  $v_{xd} = (1 - c_{mb})(v_2 - v_3)$ ,  $d_s$  - Diameter of sand, m.

The pressure gradient differential equation can be expressed as:

friction coefficient:

$$\tau_1 = \frac{1}{8} f_1 \rho_1 v_1^2 \quad (22)$$

$$\tau_2 = \frac{1}{8} f_2 \rho_2 v_2^2 \quad (23)$$

$$\tau_3 = \frac{1}{2} \eta (\rho_s - \rho_m) g c_{mb} d_s \quad (24)$$

The sliding friction coefficient can be calculated by the following formula:

$$\eta = \eta_0 (1 + 0.043 \text{Re}_{wm}^{0.6142}) \quad (25)$$

The Reynolds number expression of the multiphase mixture in the perforation is:

$$\text{Re}_{wm} = \frac{(q_{so} \rho_o + q_{sw} \rho_w)(q_{so} + q_{sw})}{\pi (q_{so} \mu_o + q_{sw} \mu_w)} \quad (26)$$

The wall friction coefficient and the flow are different in the laminar and turbulent states. [34] When the flow is laminar,

$$f_1 = f_{01} (1 + 0.043 \text{Re}_{wm}^{0.6142}) \quad (27)$$

$$f_2 = f_{02} (1 + 0.043 \text{Re}_{wm}^{0.6142}) \quad (28)$$

Calculation formula for laminar flow coefficient of conventional circular tube flow:

$$f_{01} = \frac{64}{\text{Re}_1} \quad (29)$$

$$f_{02} = \frac{64}{\text{Re}_2} \quad (30)$$

When the flow in the wellbore is turbulent, the prediction effect of the turbulent wall friction coefficient of the perforated pipe given in the Ouyang pressure drop model has higher accuracy than other models. [35]

$$f_1 = f_{01} (1 - 0.0153 \text{Re}_{wm}^{0.3978}) \quad (31)$$

$$f_2 = f_{02} (1 - 0.0153 \text{Re}_{wm}^{0.3978}) \quad (32)$$

Calculation formula for friction coefficient of conventional circular pipe turbulent flow wall: [36]

$$f_{01} = 0.0184 \text{Re}_1^{-0.2} \quad (33)$$

$$f_{02} = 0.0184 \text{Re}_2^{-0.2} \quad (34)$$

$$\text{Re}_1 = \frac{\rho_1 v_1 d_1}{\mu_1} \quad (35)$$

$$\text{Re}_2 = \frac{\rho_2 v_2 d_2}{\mu_2} \quad (36)$$

The hydraulic diameter calculation formula is:

$$d_1 = \frac{4A_1}{s_1 + s_{12}} \quad (37)$$

$$d_2 = \frac{4A_2}{s_{12} + s_2 + s_{23}} \quad (38)$$

Mixing viscosity of oil-water two-phase:

$$\mu_1 = \mu_o (1 - \alpha_{w1})^{-2.5} \quad (39)$$

$$\mu_2 = \mu_w (1 - \alpha_{o2})^{-2.5} \quad (40)$$

Interfacial friction coefficient between two liquid layers. [37]

$$f_i = \begin{cases} f_1 & (v_1 > v_2) \\ 0 & (v_1 = v_2) \\ f_2 & (v_1 < v_2) \end{cases} \quad (41)$$

$$\rho_i = \begin{cases} \rho_1 & (v_1 > v_2) \\ 0 & (v_1 = v_2) \\ \rho_2 & (v_1 < v_2) \end{cases} \quad (42)$$

The expression of the frictional stress between the layered flowing liquid layer and the sand bed:

$$\tau_{23} = \frac{1}{8} f_i \rho_i (v_2 - v_3)^2 \quad (43)$$

Since the liquid layer flow rate is definitely faster than the sand bed layer:

$$f_{23} = \left( 3.14 + 2 \lg \frac{d_2}{d_3} \right)^{-2} \quad (44)$$

#### 4.3. Decentralized Flow

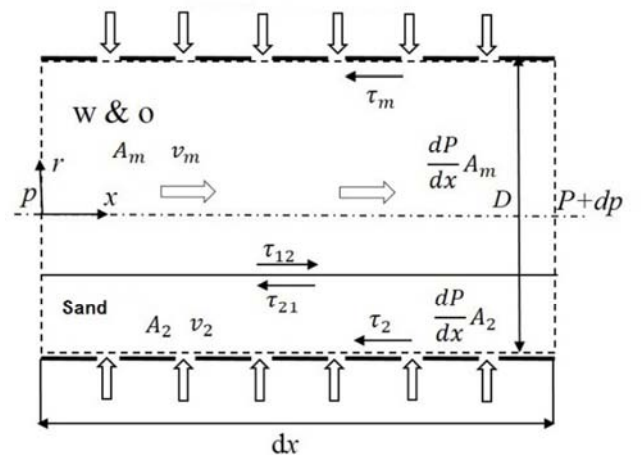


Figure 14. Control body of dispersed flow.



The continuation equation for the stratification of the flow:

$$\frac{dq_m}{dx} = q_{sm} \quad (45)$$

$$\frac{dq_s}{dx} = q_{ss} \quad (46)$$

The liquid volume flow rate calculation formula is:

$$q_m = q_o + q_w \quad (47)$$

Liquid phase flow rate:

$$v_m = \frac{q_m}{A_1} \quad (48)$$

So:

$$\frac{dv_m}{dx} = \frac{q_{sm}}{A_1} \quad (49)$$

$$\frac{dv_s}{dx} = \frac{q_{ss}}{A_1} \quad (50)$$

Assuming that the sand bed has a moving speed, the momentum conservation equation for the liquid phase mixed layer and the sand bed layer is assumed, and assuming that the wall wall injection angle is 90 degrees and the momentum correction coefficient is 1, the following are:

$$-\frac{d(pA_1)}{dx} - \tau_{1s_1}(1-\phi) - \tau_{12}s_{12} = \frac{d(\rho_m A_1 v_m^2)}{dx} \quad (51)$$

$$-\frac{d(pA_2)}{dx} - \tau_{2s_2}(1-\phi) + \tau_{12}s_{12} = \frac{d(\rho_s A_2 v_s^2)}{dx} \quad (52)$$

Equations (51) and (52) are subtracted from the constraint equation of oil-water dispersion flow:

$$(1-\phi)\left(\frac{\tau_{2s_2}}{A_2} - \frac{\tau_{1s_1}}{A_1}\right) - \tau_{12}s_{12}\left(\frac{1}{A_1} + \frac{1}{A_2}\right) = 2\left(\rho_m A_1 \frac{dv_m}{dx} - \rho_s A_2 \frac{dv_s}{dx}\right) \quad (53)$$

Adding the above two formulas, the equation for calculating the pressure drop of the oil-water-carrying sand-dispersing flow wellbore can be obtained:

$$-\frac{dp}{dx} A = 2\left(\rho_m A_1 \frac{dv_m}{dx} + \rho_s A_2 \frac{dv_s}{dx}\right) + (1-\phi)(\tau_{1s_1} + \tau_{2s_2}) \quad (54)$$

Considering the additional pressure generated by the fluid flow in the sand bed, the above formula can be:

$$-\frac{dp}{dx} A = 2\left(\rho_m A_1 \frac{dv_m}{dx} + \rho_s A_2 \frac{dv_s}{dx}\right) + (1-\phi)(\tau_{1s_1} + \tau_{2s_2}) + A_2 \frac{\rho_l c_{mb} v_{xds}^2}{d_s (1-c_{mb})^{4.8}} \left[\frac{17.3}{Re_f} + 0.336\right] \quad (55)$$

$$\rho_l = \rho_o(1-c_w) + \rho_w c_w \quad (56)$$

$$\rho_m = \rho_s c_s + \rho_l(1-c_s) \quad (57)$$

$$\tau_1 = \frac{1}{2} \rho_m |v_m| v_m f_1 \quad (60)$$

Shear stress between the suspension layer and the sand bed:

$$\tau_{12} = \frac{1}{2} \rho_m |v_m - v_s| (v_m - v_s) f_{12} \quad (61)$$

The fluid Reynolds number  $Re_f = \frac{\rho_m v_m d_1}{\mu_m}$

Hydraulic diameter of suspension layer  $d_1 = \frac{4A_1}{s_1 + s_{12}}$

Effective viscosity of suspension layer:

$$\mu_m = \mu_l (298.26c_s^3 - 45.098c_s^2 + 2.7484c_s + 1) \quad (58)$$

$$f_1 = \alpha_h Re_h^{-\beta_h} \quad \alpha_h = 0.046 \quad \beta_h = 0.02 \quad (62)$$

Relative velocity

$$v_{xds} = (1-c_{mb})(v_m - v_s) \quad (59)$$

Reynolds number of layer suspension:

$$Re_h = \frac{\rho_m v_m d_1}{\mu_m} \quad (63)$$

Shear stress between the oil-water sand suspension layer and the wellbore wall:

The critical moisture content of the phase transition of the oil-water two-phase mixture is calculated by the following

formula.

$$\eta_{cr} = \frac{1}{1 + \left(\frac{\mu_o}{\mu_w}\right)^{0.4} \left(\frac{\rho_o}{\rho_w}\right)^{0.6}} \quad (64)$$

Coefficient of friction between the suspension layer and the sand bed:

$$\frac{1}{\sqrt{2f_{12}}} = -0.86 \left[ \frac{\frac{d_s}{d_1}}{3.7} + \frac{2.51}{\text{Re}_h \sqrt{2f_{12}}} \right] \quad (65)$$

Shear force between moving bed and sand bed:

$$\tau_{23} = \frac{1}{2} f_{12} \rho_2 |v_2| v_2 \quad (66)$$

Shear force between the moving bed and the wall of the wellbore:

$$\tau_2 = \frac{1}{2} f_2 \rho_2 |v_2| v_2 \quad (67)$$

Coefficient of friction between the moving bed and the wall of the wellbore:

$$f_2 = 0.046 \text{Re}_2^{-0.02} \quad (68)$$

Reynolds number

$$\text{Re}_2 = \frac{\rho_2 v_2 d_2}{\mu_2} \quad (69)$$

Hydraulic equivalent diameter:

$$d_2 = \frac{4A_2}{s_{12} + s_2} \quad (70)$$

Mixing viscosity of moving sand bed:

$$\mu_m = \mu_l \left( 298.26 c_{mb}^3 - 45.098 c_{mb}^2 + 2.7484 c_{mb} + 1 \right) \quad (71)$$

Effective density of moving bed:

$$\rho_2 = \rho_s c_{mb} + \rho_l (1 - c_{mb}) \quad (72)$$

#### 4.4. Programming Calculation

When programming, it is necessary to first determine the flow state of the fluid, and then select the corresponding calculation model according to the flow state to calculate the pressure drop and related parameters.

The flow state is judged on the basis of the dispersion flow stability criterion. According to the Torres-Monzon model, [38] the calculation of the maximum droplet diameter and critical spherical diameter of the oil-water dispersion flow is

the core of the dispersion stability criterion. Among them, the balance between the turbulent pulse dynamics and the interfacial tension is the key factor determining the maximum droplet diameter of the dispersed flow.

The dimensionless maximum droplet diameter:

$$\tilde{d}_{l\max} = \frac{d_{l\max}}{D} \quad (73)$$

Maximum droplet diameter:

$$d_{l\max} = \frac{0.55}{We^{0.6} f_c^{0.4}} \quad (74)$$

The Weber number of the continuous phase in the liquid phase mixed dispersion system, dimensionless. [39]

$$We = \frac{\rho_c v_m^2}{\sigma_{ow}} D \quad (75)$$

Wall friction coefficient of continuous phase in liquid phase mixed flow system:

$$f_c = \frac{0.046}{\text{Re}_c^{0.2}} \quad (76)$$

Reynolds number of continuous phase in liquid phase mixed flow system

$$\text{Re}_c = \frac{\rho_c v_m D}{\mu_c} \quad (77)$$

If the dispersed flow system is water-in-oil  
 $\rho_c = \rho_o$   $\mu_c = \mu_o$  ;

If the dispersed flow system is oil-in-water  
 $\rho_c = \rho_w$   $\mu_c = \mu_w$  .

The dispersed phase in the liquid phase mixing system will have a certain influence on the maximum droplet diameter, if this effect is considered. [40]

$$\tilde{d}_{l\max} = \left( \frac{c_c}{1 - c_c} \right)^{0.6} \frac{2.22}{We^{0.6} f_c^{0.4}} \quad (78)$$

If the water is a dispersed phase  $c_c = c_w$  ;

If the oil is a dispersed phase  $c_c = 1 - c_w$  .

Critical spherical diameter:

$$\tilde{d}_{cr} = \frac{1.265}{Eo^{0.5}} \quad (79)$$

Eotvos number of liquid mixed flow system, dimensionless:

$$Eo = \frac{g(\rho_w - \rho_o) D^2}{\sigma_{ow}} \quad (80)$$

The liquid phase mixed dispersion flow stability criterion is

expressed as:

$$\tilde{d}_{l\max} \leq \tilde{d}_{cr} \quad (81)$$

The minimum energy method is explained below: Two types of energy values are considered in the horizontal well section, namely kinetic energy and surface energy. [41]

$$\text{Kinetic energy: } E_k = \frac{1}{2} (A_1 \rho_1 v_1^2 + A_2 \rho_2 v_2^2) \quad (82)$$

Surface energy:

$$E_s = \sigma_{ow} \left[ D \sin \gamma_1 + 6 \left( \frac{A_1 \alpha_{w1}}{d_{sm1}} + \frac{A_2 \alpha_{o2}}{d_{sm2}} \right) \right] \quad (83)$$

Sauter mean diameter of oil-water two-phase stratified flow oil layer or water-in-oil layer, water layer or oil-in-water layer dispersed phase:

$$d_{sm1} = \frac{2 \times 10^{-8}}{v_1^2 f_{01}^{3.12}} \quad (84)$$

$$d_{sm2} = \frac{2 \times 10^{-8}}{v_2^2 f_{02}^{3.12}} \quad (85)$$

#### 4.5. Error Analysis

In this study, the pressure drop predicted by the model is compared with the measured pressure drop of the wellbore, as shown in Figure 15, where the maximum relative error in the model is 19.44% and the average relative error is 12.69%. The above-mentioned error is because of three reasons. First, the vibration of the instrument will introduce some measurement errors. Second, the pressure drop measurement system is suitable for a liquid system. Because the sealing of the equipment is not very good, bubbles often appear in the pressure tubes, and these will affect the accuracy of the measurement results. Finally, the artificial observation of the experimental phenomena also introduces errors, though overall, the results satisfy the requirements of a practical engineer.

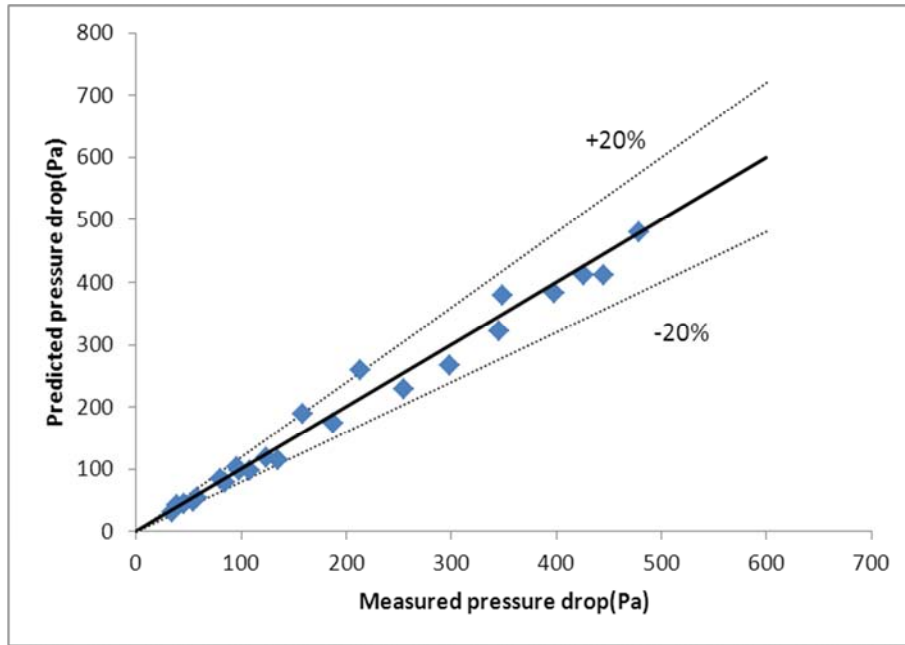


Figure 15. Measured pressure drop vs. predicted pressure drop.

## 5. Conclusions

1). With the increase in the viscosity of heavy oil, the sand-carrying capacity increases gradually. Specifically, under the condition of a constant flow rate, the larger the heavy oil viscosity, the lower the sand-bed height, but the wellbore pressure drop gradually increases with the increase in the viscosity of heavy oil.

2). With the increase in the water content, the speed of particle sedimentation increases, leading to the development of a sand-bed at the bottom of the wellbore. The moisture

content is present at the reverse phase point.

3). The influence of the wall inflow on the pressure drop of the wellbore is relatively small. With the increase in the wall inflow, the pressure drop of the wellbore increases slightly and approximately linearly.

4). In this study, the pressure drop predicted by the model is compared with the measured pressure drop of the wellbore. The maximum relative error of the model is 19.44% and the average relative error is 12.69%; these can satisfy the requirements of practical engineering.

## Acknowledgements

The author would like to thank the following projects for their supports: Offshore Oil Efficient Development National Key Laboratory's "Forecast method research of sand carrying capacity in the wellbore of high angles wells" (CCL2013RCPS0239GNN) and the National Natural Fund Project "Flowing law research of oil-gas-water-sand complex flow in the horizontal wellbore" (51474225).

## Nomenclature

subscript 1 oil or water-in-oil layer  
 subscript 2 water oil-in-water layer  
 subscript 3 movable sand-bed or fixed sand-bed  
 $v_1$  velocity of oil or water-in-oil flow, m/s  
 $v_2$  velocity of water or oil-in-water flow, m/s  
 $v_3$  velocity of sandbed flow, m/s  
 $C_{mb}$  sand volume concentration, dimensionless  
 $\tau_2$  shear stress between the water layer and wall, Pa  
 $\tau_1$  shear stress between the oil layer and wall, Pa  
 $\tau_3$  shear stress between the sand-bed layer and water layer, Pa  
 $\tau_{12}$  shear stress between the oil or water-in-oil layer and water or oil-in-water layer, Pa  
 $\tau_{23}$  shear stress between the sand-bed and water or oil-in-water layer, Pa  
 $D$  wellbore diameter, m  
 $\Delta P / L$  pressure gradient, Pa/m  
 $C_w$  mixture water content, dimensionless  
 $C_o$  mixture oil content, dimensionless

## References

- [1] Wang, Zhi-Ming., Jin, HUI., Wei, Jian-Guang., 2009, "Research on coupled model of horizontal well fractures variable mass influx and reservoir seepage", Chinese Journal of Hydrodynamics. 24 (2): 172-178.
- [2] Sun, J. P., 2005, "Study on Mechanism of Sand Production by Sand in Heavy Oil Reservoir of Loose Sandstone," Southwest Petroleum Institute.
- [3] Ehlig-Economides, C. A., Fernandez, B. G., Gongora, C. A., 2000, "Global experiences and practice for cold production of moderate and heavy oil," SPE58773.
- [4] Frederic, G., 2007, "Optimization of well performance in a selective subsea sand-control completion offshore Nigeria," SPE98226.
- [5] Asheim, H., Kolnes, J., Oudeman, P. A., 1992, "Flow resistance correlation for completed wellbore," Journal of Petroleum Science and Engineering. 8: 97-104.
- [6] Novy, P. A., 1995, "Pressure drop in horizontal wells: when can they be ignored". SPE Reservoir Engineering, 2: 29-35.
- [7] Su, Z., Gudmundsson, J. S., 1998, "Perforation inflow reduces frictional pressure loss in horizontal wellbores," Journal of Petroleum Science and Engineering, 19: 223-232.
- [8] Su, Z., Gudmundsson, J. S., 1994, "Pressure drop in perforated pipes: experiments and analysis," SPE28800: 563-574.
- [9] Su, Z., Gudmundsson, J. S., 1993, "Friction factor of perforation roughness in pipes," SPE26521: 151-163.
- [10] Su, Z., 1992, "Influence of wellbore hydraulics on horizontal well pressure transient behavior," SPE24684: 255-264.
- [11] Ihara, M., Brill, J. P., Shoham, O., 1992, "Experimental and theoretical investigation of two-phase flow in horizontal wells," SPE 24766: 57-67.
- [12] Ihara, M., Yanai, K., Yakao, S., 1995, "Two-phase flow in horizontal wells," SPE Production & Facilities, 11: 249-255.
- [13] Ihara, M., Shimizu, N., 1993, "Effect of accelerational pressure drop in a horizontal wellbore," SPE 26519: 125-138.
- [14] Ihara, M., Kikuyama, K., Hasegawa, Y., 1994, "Flow in horizontal wellbores with influx through porous walls," SPE28485: 225-235.
- [15] Plaxton, B. L., 1995, "Pipe flow experiments for the analysis of pressure drop in horizontal wells," SPE International Student Paper Contest, 11: 635-650.
- [16] Yuan, H., Sarica, C., Brill, J. P., 1996, "Effect of perforation density on single phase liquid flow behavior in horizontal wells," The 1996 International Conference on Horizontal Well Technology Held in Calgary, Canada: Alberta, November: 603-612.
- [17] Yuan, H., 1995, "Investigation of single phase liquid flow behavior in horizontal wells," Fluid Flow Projects Advisory Board Meeting, The University of Tulsa: 103-117.
- [18] Yuan, H., Sarica, C., Brill, J. P., 1998, "Effect of completion geometry and phasing on single-phase liquid flow behavior in horizontal wells," SPE48937: 93-104.
- [19] Yuan, H., Sarica, C., Miska, S., 1997, "An experimental and analytical study of single-phase liquid flow in a horizontal well," Journal of Energy Resources Technology: 119 (3): 20-25.
- [20] Ouyang, L. B., Arbabi, S., Aziz, K., 1996, "General wellbore flow model for horizontal vertical and slanted well completions," The 1996 SPE Annual Technical Conference, October: 349-361.
- [21] Ouyang, L. B., Aziz, K., 2000, "A homogeneous model for gas-liquid flow in horizontal wells," Journal of Petroleum Science and Engineering, 27 (3): 119-128.
- [22] Ouyang, L. B., Aziz, K., 1999, "A mechanistic model for gas-liquid flow in pipes and wells," SPE 56525: 359-372.
- [23] Schulkes, R., Utvik, O. H., Rinde, T., 1997, "Pressure drop in horizontal wells: multiphase flow with radial inflow," BHR Group Multiphase: 45-55.
- [24] Zhou, S. T., Zhang, Q., Li, M. Z., 1998, "Experimental research on horizontal well variable mass flow," Journal of University of petroleum, 22 (5): 53-55.
- [25] Wang, X. Q., 2004, "Research on horizontal well and reservoir coupled variable mass flow rules," BeiJing: China University of Petroleum.

- [26] Xue, L., Wang, Z. M., Wang, X. Q., 2006, "Research on influence rules of injection ratio on horizontal well pressure drop," *Journal of China University of Petroleum (Natural Sciences)*, 30 (4): 71-74.
- [27] Wang, X. Q., Wang, Z. M., Wei, J. G., 2005, "Research on wellbore and reservoir horizontal well coupled variable mass flow rules," *Chinese Journal of Hydrodynamics A*, 20 (3): 326-331.
- [28] Wang, Z. M., Jin, H., Wei, J. G., 2009, "Research on coupled model of horizontal well fractures variable mass influx and reservoir seepage," *Chinese Journal of Hydrodynamics*, 24 (2): 172-178.
- [29] Islam, M. R., Chakma, A., 1990, "Comprehensive physical and numerical modeling of a horizontal well," *SPE20627*: 111-123.
- [30] Zhou, S. T., Zhang, Q., Li, M. Z., 2000, "Experimental research on influences of perforation inflow on horizontal well flow," *Experimental Mechanics*, 15 (3): 306-311.
- [31] Wang, X. Q., Xu, J., Wang, Z. M., 2005, "Research progress of horizontal well variable mass flow," *Natural Gas Industry*. 25 (4): 92-94.
- [32] Grigg, N. S. 1970, "Motion of single particles in alluvial channels," *J. Hyd. Div*, 96 (NY12): 2501-2518.
- [33] Lane, E. W., Kalinske, A. 1941, "Engineering Calculations of Suspended Sediment," *Trans, Amer. Geophys. Union*, 603-607.
- [34] Ranga. Raju, K. G., R. J., Garde, R. C. Bhardwaj., 1981, "Total load transport in alluvial channels," *J. Hyd. Div*. 107 (NY2): 179-192.
- [35] Salehi, S., Nygaard, R., 2015, "Full Fluid-solid Cohesive Finite-Element Model To Simulate Near Wellbore Fractures," *Journal of Energy Resources Technology*. 137 (1): 103-114.
- [36] Al-lababidi, S.; Yan, W., Yeung, H., 2012, "Sand Transportations and Deposition Characteristics in Multiphase Flows in Pipelines," *Journal of Energy Resources Technology*. 134 (3): 45-58.
- [37] Barrios, L., Prado, M. G., 2009, "Experimental Visualization of Two-Phase Flow Inside an Electrical Submersible Pump Stage," *Journal of Energy Resources Technology*. 133 (4): 74-82.
- [38] King, M. J. S., Farhurst, C. P., and Hill, T. J., 2000, "Solids Transport in Multiphase Flows Application to High Viscosity Systems," *Energy Sources Technology Conference*, New Orleans, pp. 14-17.
- [39] Barrios, L., Prado, M. G., 2009, "Modeling Two-Phase Flow Inside an Electrical Submersible Pump Stage," *Journal of Energy Resources Technology*. 133 (4): 144-157.
- [40] Adesina, Fadairo A. S., Churchill, A., Olugbenga, F., 2011, "Modeling Productivity Index for Long Horizontal Well," *Journal of Energy Resources Technology*. 133 (3): 55-64.
- [41] Qian, N., Wan, Z. H., 1998, "Mechanical Mechanics of Sediment," Beijing: Science Press, 139-148.